LEGIBILITY NOTICE

A major purpose of the Technical Information Center is to provide the broadest dissemination possible of information contained in DOE's Research and Development Reports to business, industry, the academic community, and federal, state and local governments.

Although a small portion of this report is not reproducible, it is being made available to expedite the availability of information on the research discussed herein.

LA-UR -90-1999

Los Alamos National Laboratory is operated by the University of California for the United States Department of Energy under contract W-7405-ENG-36

LA-UR--90-1999

DE90 013175

TITLE Line-imaging Fabry-Perot interferometer

AUTHOR(S)

A. R. Mathews
R. H. Warnes
W. F. Hemsing
G. R. Whittemore

SUBMITTED TO

SPIE
Optical and Optoelectronic Applied Science and Engineering
San Diego, California July 8-13, 1990

DISCLAIMER

Los Alamos Los Alamos National Laboratory
Los Alamos, New Mexico 87545

Line-imaging Fabry-Perot interferometer

A.R. Mathews, R.H. Warnes, W.F. Hemsing, and G.R. Whittemore *

Los Alamos National Laboratory, MS P940
Los Alamos, NM 87545 USA

ABSTRACT

A method for measuring the velocity history of a line element on a shock-loaded solid has been demonstrated. Light from a single-frequency laser is focused through a cylindrical lens to a line on a moving target. The return Doppler-shifted image is passed through a Fabry-Perot interferometer. Because only specific combinations of incident light angle and frequency can pass through the interferometer, the output is an incomplete image of the moving target appearing as a set of fringes. This image is focused onto an electronic streak camera and swept in time. The fringe pattern changes with time as the target surface moves, allowing determination of velocity for each point on the target that forms a fringe. Because the velocity can only be measured at the fringe positions, it is necessary to use an interpolating polynomial to obtain a continuous function of time and velocity along the sampled line.

1. INTRODUCTION

Since the late 1960s, shockwave physicists have used optical techniques such as VISAR and Fabry-Perot (FP) interferometry to measure the velocity history of an explosively driven target. In both techniques, a laser illuminates a spot on the moving surface, and the frequency of the Doppler-shifted return light gives a measure of the velocity. Review articles by McMillan, et al. [1], and Barker [2] describe the theory and use of interferometers for measuring the velocity as a function of time for a single point. A recent paper by Gidon and Behar [3] presents a technique for measuring the instantaneous velocity as a function of position for an entire surface.

In this paper we describe a method, based on Fabry-Perot interferometry, for determining the continuous velocity history of a line segment on a fast moving surface. The idea was originally proposed by John Corfe of AWE, Aldermaston, U.K. [4], who fielded experiments to test the validity of the technique. We have performed similar experiments and have developed computer programs to quantitatively analyze the results.

2. DISCUSSION OF THE METHOD

In a typical FP experiment, a spherical lens focuses light from a single-frequency laser onto a spot on the moving target, which must be near the focal point of the lens. Reflected light is collected and nearly collimated by this lens and directed into the interferometer. The FP will transmit light that is incident at only a discrete set of angles from the interferometer axis. These favored angles are determined by the wavelength of the light and the FP mirror spacing. Light exiting the FP is collected by another spherical lens, and a fringe pattern is formed in the focal plane of this lens. When properly aligned, the pattern is a set of concentric rings of high finesse.

*This work was supported by the United States Department of Energy under contract number W-7405-ENG-36.

The mathematical analysis of the fringe pattern is discussed in many standard optics texts. We will follow the notation of Born and Wolf [5] to highlight some of the important relations. Light rays exiting the FP interfere constructively when the interference condition

$$m\lambda = 2d\cos\theta \tag{1}$$

is met. In this equation, m is the (integer) fringe order, λ is the wavelength of the light, d is the FP mirror spacing, and θ is the angle of incidence of the light measured with respect to the mirror axis. When a lens of focal length f brings the rays to a focus, bright rings will appear at radii given by

$$r_m = f\tan\theta_m \simeq f\theta_m \ . \tag{2}$$

The order of the central ring ($\theta = 0$) is given by

$$m_0 = \frac{2d}{\lambda} \tag{3}$$

so,

$$m = m_0\cos\theta_m \simeq m_0\left(1 - 2\sin^2\frac{\theta_m}{2}\right) \ . \tag{4}$$

Thus, for small angles,

$$\theta_m \simeq \sqrt{\frac{2(m_0 - m)}{m_0}} \ . \tag{5}$$

Because the fringe order for the central ring is usually not an integer, it is normal to write the order for the first bright ring in terms of a fractional order, e, as

$$m_1 = m_0 - e \qquad 0 < e < 1 \ . \tag{6}$$

Then, the order for the pth bright ring (measured from the center) is given by

$$m_p = m_0 - e - (p-1) \ . \tag{7}$$

Combining Eqs. (2), (5) and (7), gives the radius of the pth ring:

$$r_p^2 \simeq f^2\frac{2(m_0 - m_p)}{m_0} = \frac{f^2}{d}[(p-1) + e] \ . \tag{8}$$

Thus a frequency shift caused by motion of the target will lead to a change in the radii of all the circular fringes. Because each fringe originates from the same illuminated spot on the target, a typical multi-fringe pattern contains redundant velocity information. By measuring the radii of these fringes as a function of time, a precise velocity history for one point on the target can be determined.

For dynamic experiments, a major diameter of the circular fringe pattern is usually projected onto the slit of a high-speed electronic streak camera. The resulting film record has the following characteristics:

a) Portions of the record corresponding to constant velocity appear as straight lines parallel to the time axis.

b) Acceleration of the target toward the source causes the circular fringes to move outward, occasionally spawning new fringes at the center of the pattern.

c) All fringes are symmetric about the center of the pattern.

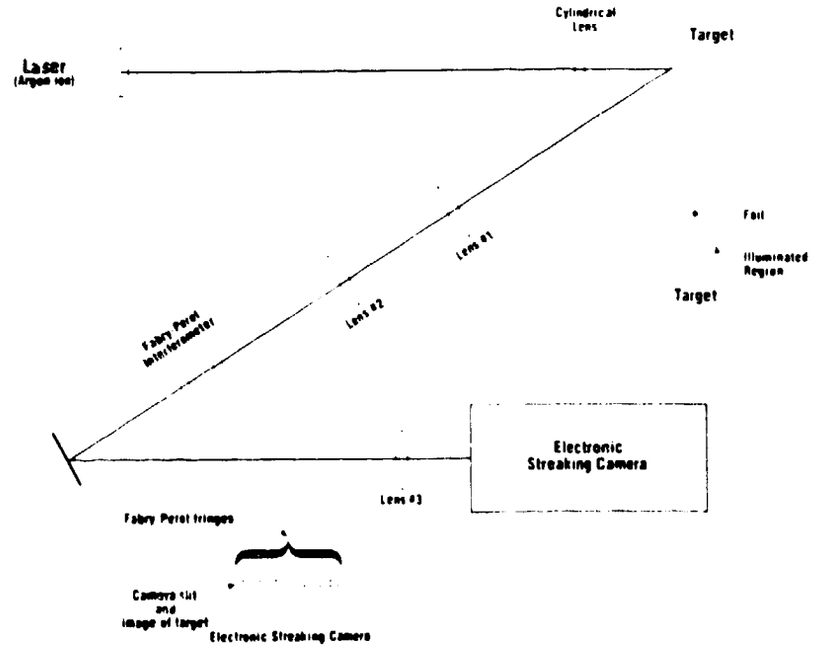

Fig. 1. Experimental setup for the line Fabry-Perot interferometer.

In the line-imaging version of the FP interferometer, we pass light from a 3 Watt CW argon-ion laser ($\lambda = 514.5$ nm) through a cylindrical lens to illuminate a 3.0-mm line segment on the target surface. For the experiments described here, the target is a thin plastic sheet driven by an electrically exploded copper foil. We expect the resulting velocity profile to be zero at the edges and rise to a maximum of 3 or 4 km/s at the center. The width and flatness of the velocity peak varies from one experiment to another. Figure 1 illustrates the experimental arrangement.

The light from the illuminated line on the target is collected and nearly collimated by one or two spherical lenses, and directed to the FP. These two lenses, in conjunction with the spherical lens at the output of the FP, determine the size of the image on the streak camera slit. The FP acts as a spatial filter, transmitting only the light that enters at the preferred set of angles (again, determined by the wavelength of the light and the FP mirror spacing). For the line FP, the light collected from the target originates from many points along the illuminated line. Thus, for a given mirror spacing, the image on the camera slit will be a set of bright fringes at positions where the input angle and the wavelength of the light permit transmission through the FP. We then streak the image in time (total time ≈ 1 μs) and record the fringes on film.

In the line-imaging FP, there is no redundant velocity information; a fringe in the slit plane gives information about the target velocity only at the corresponding position on the target. There is no velocity information between fringes. If the target is stationary, or moving at a constant velocity, the fringe pattern will consist of a set of concentric rings spaced similarly to those in a point FP record.

As the target accelerates, the wavelength of the reflected light will change, and the conditions for constructive interference will also change. Changes in wavelength combined with different input angles across the target lead to distortions in the fringe pattern in regions with relatively larger or smaller acceleration.

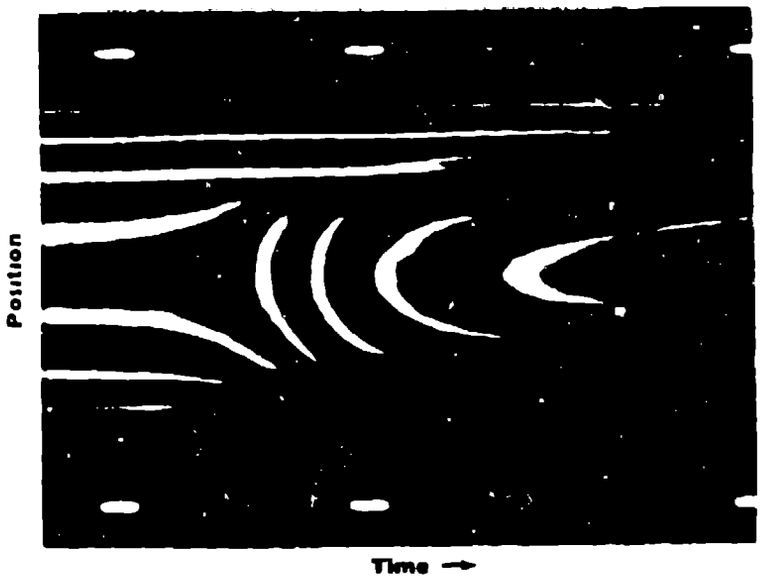

Fig. 2. Grayscale display of the digitized streak camera record. The illuminated line is oriented vertically and time is increasing to the right. Note that the fringes are not symmetrical about the center of the pattern.

An example of the resulting line FP streak record is shown in Fig. 2. Measurement of the fringe locations provides a measure of the target velocity as a function of time at discrete positions along the illuminated line.

3. VELOCITY CALCULATION

The mathematical analysis required to convert fringe location to velocity is straightforward and is equivalent to that for a point FP interferometer. It can be shown [1,3] that the velocity for the nth dynamic fringe is given by

$$v = \frac{c\lambda}{4d}\left(\frac{r^2 - r_0^2}{r_1^2 - r_0^2} - n\right), \tag{9}$$

where

n = *dynamic fringe number, increasing outward from the center of the pattern* $(n = p - 1)$,
r_0 = *radius of the innermost static fringe,*
r_1 = *radius of the next larger static fringe,*
r = *radius of a dynamic fringe, and*
c = *velocity of light.*

The term $(c\lambda / 4d)$, the "fringe constant," is the velocity change required to displace a fringe, number n, to the position of the next larger fringe, number $n + 1$. The first term in parenthesis in Eq. (9) is the partial fringe displacement from the static position to the dynamic position, r. The second term, n, is the fringe number for a static fringe that has been displaced to a new dynamic position. It allows for integer

fringe discontinuities that can occur in some experiments. The value of n increases by one for each fringe counted outward from the innermost fringe ($n = 0$). As new fringes are born, however, the value of n associated with the fringe becomes less than zero and decreases by one for each new fringe.

If we now define

$$a = \frac{c\lambda}{4d\,(r_1^2 - r_0^2)}$$

and

$$b = \frac{c\lambda}{4d}\left(\frac{r_0^2}{r_1^2 - r_0^2} + n\right) ,$$

then Eq. (9) can be rewritten in the form

$$v = ar^2 - b . \tag{10}$$

Thus, a plot of velocity as a function of radius shows that solutions to Eq. (9) describe a set of parabolas separated by constant distance along the $r = 0$ axis. These parabolas represent the locations that bright fringes will form for any combination of velocity and position [6]. Plotting the intersections between the parabolas and the assumed velocity profile gives the positions of fringes for any given time, t. If this process is repeated for many different values of t, a synthetic streak record for the proposed experiment can be produced.

Figure 3 shows how one can predict the fringe record for the type of velocity profiles we expect in our experiments. In the upper graph the assumed velocity profiles for four different times are superimposed on the solutions to the velocity equation. Note that for $t = 0$, the static case, the velocity profile is a straight line at $v = 0$. Intersections of this velocity profile with the parabolas give the initial locations of bright fringes on the streak record. Repeating this process for three additional times produces the synthetic fringe record shown in the lower portion of Fig. 3.

Because the fringes represent the velocity at different points on the target, the dynamic portion of the record is generally not symmetric. As a result, fringes can appear and disappear in a confusing manner. A preliminary graphical analysis has made it possible for us to resolve apparent ambiguities in the physical record, and has simplified the processing necessary for quantitative analysis.

4. DATA ANALYSIS

The analysis of a fringe record is the inverse of the process described above. Starting with the dataset shown in Fig. 2, we can use the fringe position at each time to determine the velocity of the target at the corresponding location on the illuminated line. Combining the time slices yields a map of the velocity distribution as a function of time and position on the target. Because the velocity can be found only at the fringe locations, the function must be interpolated to form a continuous distribution. Details of our analysis follow.

The first step in the analysis process consisted of digitizing the film record. For our initial experiments, the useful portion of the 4x5-inch film was scanned on a flatbed microdensitometer in 30 μm increments. This yielded a digitized image with 1333 x 667 pixels that was scaled down to 666 x 333 for processing. The fringes were traced by hand, and the distance to the center of the pattern was calculated for each fringe position. We assumed that there were no discontinuous fringe jumps, so the value of the dynamic fringe number, n, changed by one for each fringe.

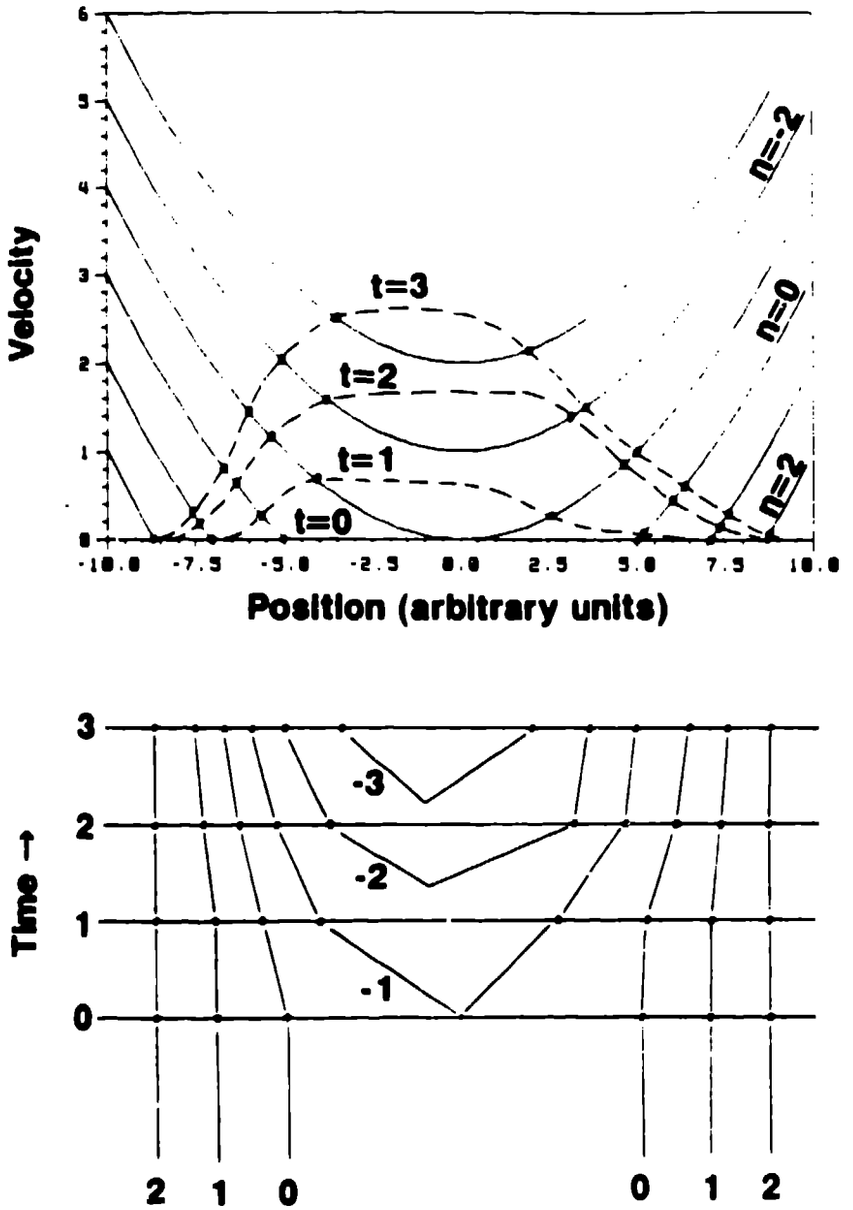

Fig. 3. Graphical representation of fringe evolution. Bright fringes occur at intersections between a velocity profile (for a given time) and parabolas that represent solutions to the velocity equation. The dotted lines in the top figure represent velocity profiles for four different times (the velocity for $t = 0$ lies along the horizontal axis). The lower half of the figure shows the fringe pattern that results from the assumed velocity profiles. Fringe number 0 is the innermost static fringe and n increases or decreases by one for each neighboring fringe. Note that new fringes are "born" between adjacent time steps.

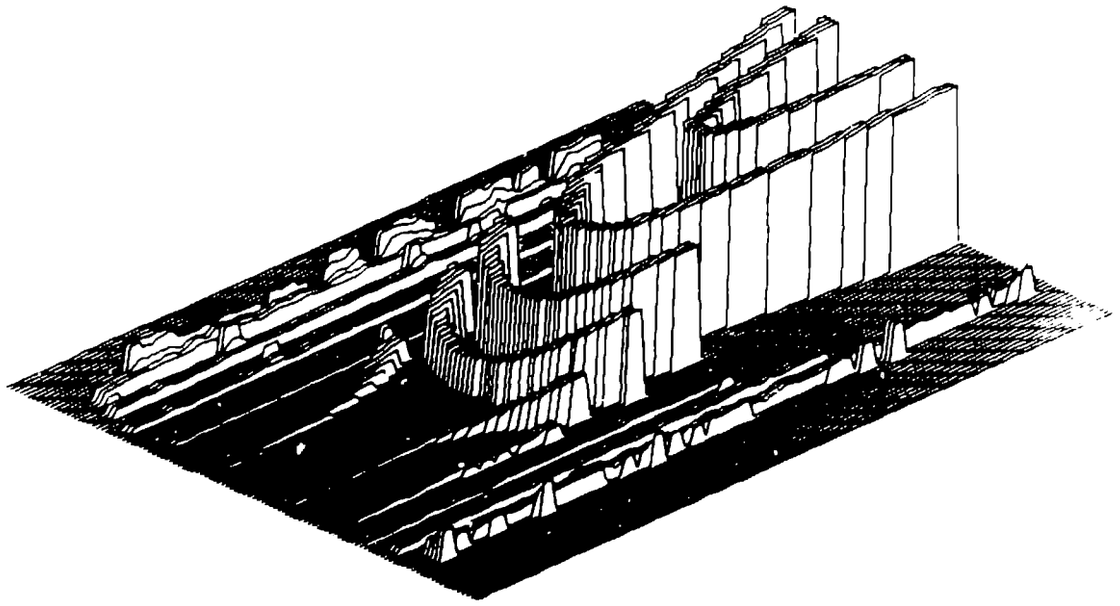

Fig. 4. The velocities calculated for each fringe position (fringe constant $\approx$ 1 km/s). The width of each fringe has been increased for easier viewing. In this graph, time is increasing toward the upper right, position is increasing toward the upper left, and velocity is increasing vertically. The time interval shown is 1 μs and the object width is approximately 3 mm.

In an attempt to reduce the errors that accompany human input (e.g., eye response, jerky hand motion), we introduced some constraints on the traced fringes. For example, the operator was given the option of allowing the program to find the maximum fringe intensity within a predefined zone surrounding the points chosen by eye. This technique was originally implemented in our point F_t analysis to reduce errors that occur because the fringe profiles are not symmetric when plotted as a function of radius. That is, the maximum intensity does not occur at the center of a fringe. In addition, the traced lines were fit with a cubic spline function to produce some smoothing (this was switched off at fringe discontinuities). We are currently investigating one- and two-dimensional fitting techniques that would automate the tracing procedure and provide subpixel accuracy. After measuring each fringe position, we used Eq. (9) to calculate the velocity as a function of time along each fringe. The resulting velocity map is shown in Fig. 4. In this presentation the fringes have been widened by a factor of five to make them more visible.

It is desirable to interpolate the velocity distribution shown in Fig. 4 to form a continuous measure of velocity as a function of time and position. Unfortunately, because there are few points per time slice, the interpolated velocity map will not be unique. The result will depend upon factors such as the choice of interpolating function, the size of the sample interval, and the noise in the measurements. We have experimented with some simple interpolation schemes that appear to preserve the shape of the data distribution while providing some smoothing for noise suppression.

The first method consists of calculating a weighted average of all non-zero velocities in a square region surrounding each pixel. We have tried varying both the size of the neighborhood and the form of the weighting function. Examples of the types of surface that result from a weighting function of the form

$1/R^p$ are shown in Fig. 5. The interpolated surface is reasonably smooth but is "pinched" in regions near the fringes. This pinching is a consequence of the enhanced weight given to nearby pixels and tends to increase as the value of p increases. That is, pixels on or near a fringe will be assigned the value of the velocity at the closest fringe (weight = 1). However, for pixels that lie between fringes, the value assigned to the pixel will be an average of velocities that are within the sample region. This leads to interpolated surfaces that peak near fringes and droop in the intervals between fringes. In general, functions with $p > 1$ lead to surfaces that conform to the data along the fringes, but drop off quickly on either side of the fringe. Weighting functions with $p \leq 1$ tend to be "stiffer," but do not follow the data values as closely.

An alternate approach consists of tiling the measured velocity distribution with planar patches and using linear interpolation between tile edges. To guarantee planar surfaces, we connect the data points with straight line segments to form triangles. A Delaunay triangulation scheme is utilized to generate non-overlapping triangles [7,8]. We then use Simplex interpolation [9] to find the value of the velocity for all points (pixels) inside each triangle.

Figures 6 and 7 demonstrate the use of this technique. Figure 6 shows the distribution of points and triangles that result for the traced dataset (reduced by a factor of 10 to make the triangles more visible). Figure 7 shows the velocity surface resulting from the Simplex interpolation between triangle vertices. This surface is more blocky than those shown in Fig. 5, but follows the data more closely. Simplex interpolation also eliminates the pinched surfaces that occur in the weighted average methods. We are investigating other interpolation schemes such as bicubic splines and thin plates, but do not expect the results to change significantly.

5. CONCLUSION

We have demonstrated that a standard point Fabry-Perot interferometer can be modified to measure the velocity of an illuminated line on a target. The resulting record is continuous in time but provides a measure of velocity only at discrete spatial positions. Because the velocity is known only at the fringe locations, and, in general, the fringes move with time, the points on the target where the velocity is known are constantly changing. Therefore, it is necessary to interpolate the reduced data to obtain a smooth map of the velocity / spatial position / time surface. Interpolation is also useful in regions where the fringes cannot be traced with confidence.

Our initial experiments yielded rather sparse data sets because we limited the number of fringes to simplify the analysis procedure. It would be straightforward, however, to modify the focal lengths of the lenses to adjust the magnification of the line target and the number of fringes superimposed on the image. Increasing the number of fringes provides a more detailed sampling of the velocity surface, but also results in a loss of precision in the measure of velocity at each fringe position.

A close examination of Fig. 2 shows evidence of anomolous fringe behavior at the edges of the object. Fringes appear to cross one another, break into fragments, or disappear completely. Our initial analysis assumes that the target acceleration is continuous in space and time, and that anomolies in the fringe record are caused by changes in the reflectivity of the target surface. Additionally, because the FP measures only a single velocity component, we assume that the dominant acceleration is parallel to the interferometer axis. These assumptions are probably not true at the edges of the object. Because the light in these regions is directed away from the interferometer, a detailed analysis is difficult.

Unfortunately, the processing techniques we have described consume large amounts of computer resources. But it is our experience that for many experiments the advantages of measuring velocity across a line on a target far outweigh the difficulties of the analysis.

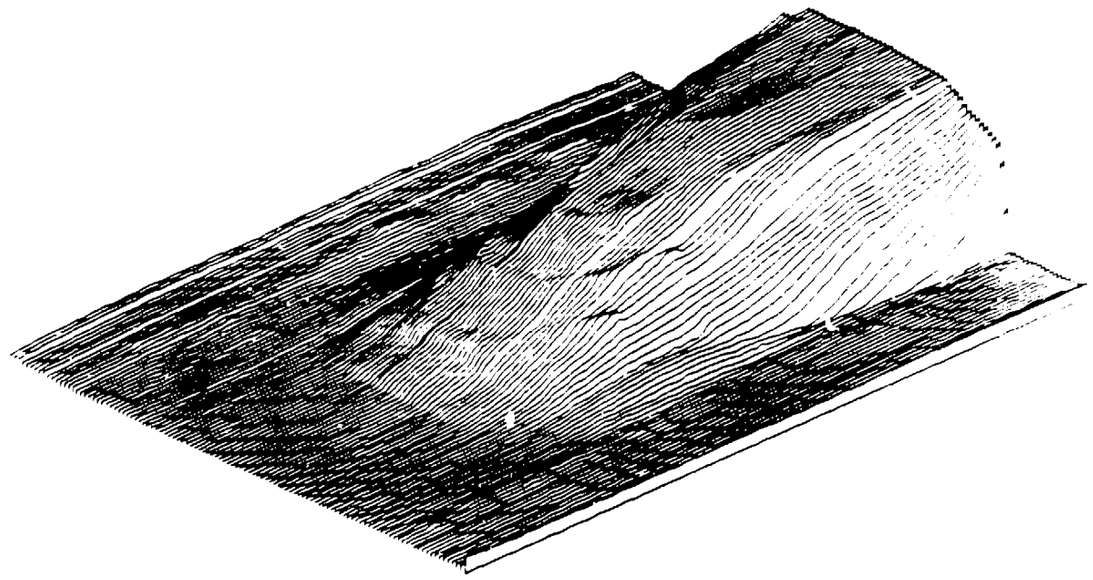

MIN = 2.011E-02 MAX = 4.063E+00 (450P X 330L, 3)

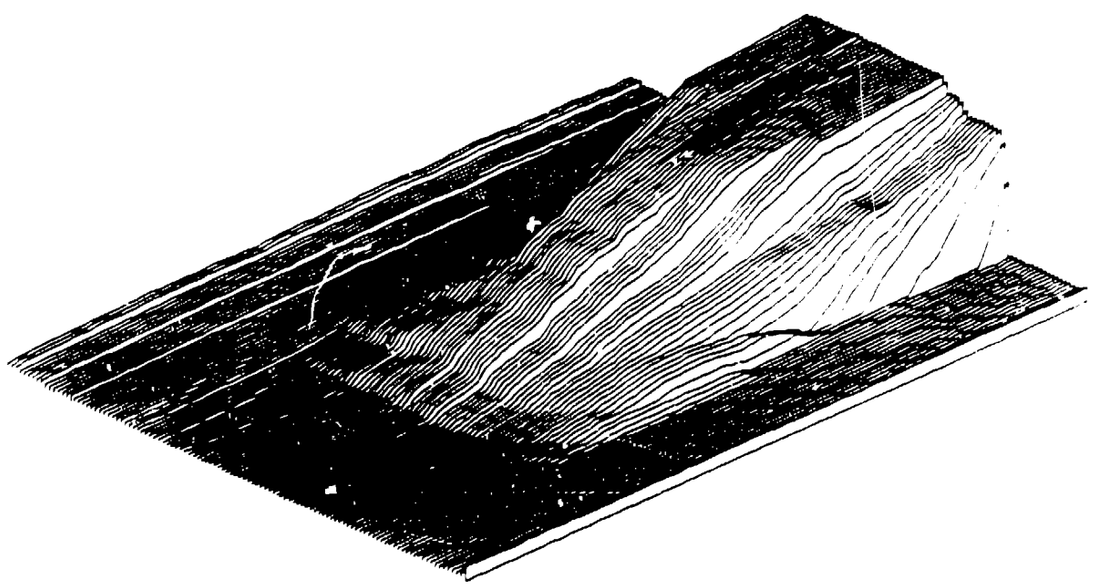

MIN = 2.213E-02 MAX = 4.064E+00 (450P X 330L, 3)

Fig. 5. The interpolated velocity distribution calculated using a weighted average of the form $1/R^p$ with p = 1.0 (upper) and p = 0. (lower). The axes and scales are the same as Fig. 4.

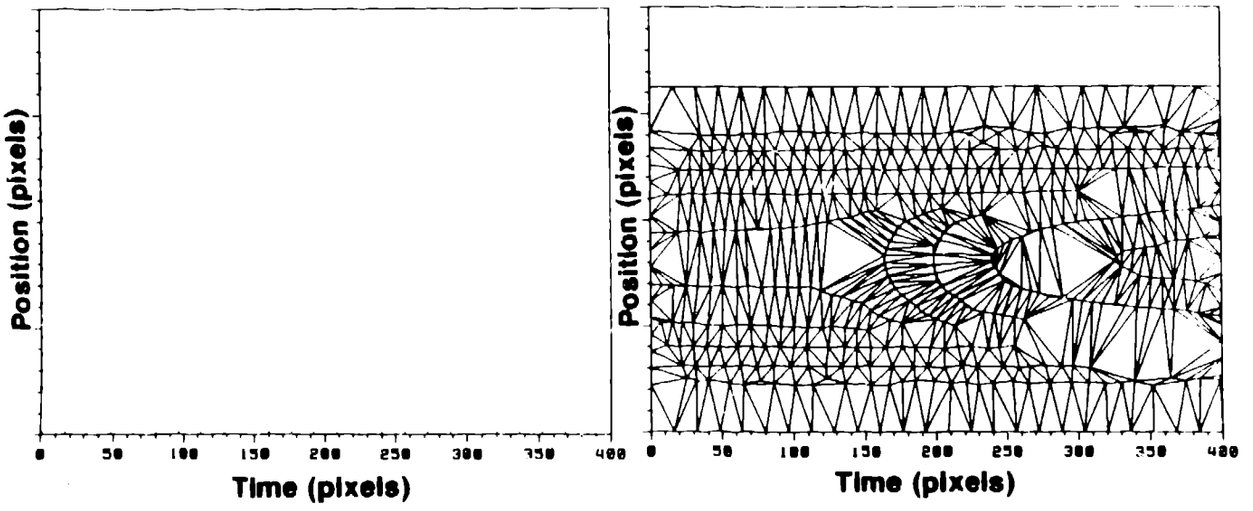

Fig. 6. Delaunay triangulation of the traced fringes. The left graph shows the traced points after reduction by a factor of 10. If the points are surrounded by a rectangular convex hull and connected, the right-hand pattern emerges.

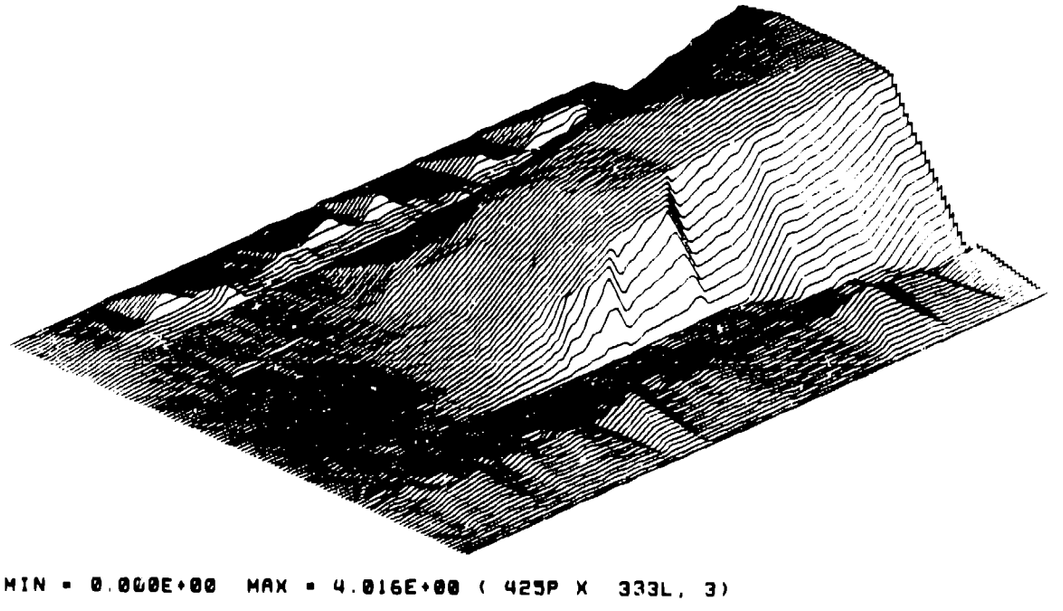

Fig. 7. Simplex interpolation of the triangulated dataset. The axes and scales are the same as Figs. 4 and 5.

References

[1] C.F. McMillan, D.R. Goosman, N.L. Parker, L.L. Steinmetz, H.H. Chau, T. Huen, R.K. Whipkey, and S.J. Perry. Velocimetry of fast surfaces using Fabry-Perot interferometry. *Rev. Sci. Instrum.*, 59:1–20, 1988.

[2] L.M. Barker. Velocity interferometry for time-resolved high-velocity measurements. In *Proceedings on High-Speed Photography, Videography and Photonics Proc. SPIE*, 427,*116*, 1983.

[3] S. Gidon and G. Behar. Instantaneous velocity field measurements: application to shock wave studies. *Applied Optics*, 25:1429–1433, 1986.

[4] J. E. Corfe. AWE, Aldermaston, U.K. Personal communication.

[5] M. Born and E. Wolf. *Principles of Optics*. Pergamon, New York, 1975.

[6] K. M. Hanson. Los Alamos National Laboratory. Personal communication.

[7] A. Maus. Delaunay triangulation and the convex hull of n points in expected linear time. *BIT*, 24:151–163, 1984.

[8] W. Eddy. A new convex hull algorithm for planar sets. *ACM Trans. on Math. Software*, 3:398–403, 1977.

[9] P.G. Ciarlet and C. Wagschal. Multipoint Taylor formulas and applications to the finite element method. *Numer. Math.*, 17:84–100, 1971.